*inorganics*

MDPI

*Article*

# Divalent Europium Complexes with Phenochalcogenato Ligands: Syntheses, Crystal Structures, and Luminescence Properties

**Zhi-Feng Wu, Qing-Song Yang, You-Song Ding * and Zhiping Zheng ***

Key Laboratory of Rare Earth Chemistry of Guangdong Higher Education Institutes, Department of Chemistry, Southern University of Science and Technology, Shenzhen 518055, China; 12232775@mail.sustech.edu.cn (Z.-F.W.); 12432173@mail.sustech.edu.cn (Q.-S.Y.)

* Correspondence: dingys@sustech.edu.cn (Y.-S.D.); zhengzp@sustech.edu.cn (Z.Z.)

**Abstract**

Divalent europium complexes have attracted significant attention in various fields due to the unique electronic configuration of the Eu(II) ion. Given the high sensitivity of the 5d → 4f emission of Eu(II) ions to the ligand field, it is crucial to explore the relationship between ligands and this emission in Eu(II) complexes. However, the heavy-atom effects on the 5d → 4f emission of Eu(II) complexes coordinated with non-metal elements in the same group remain unclear. In this study, five mononuclear Eu(II)-chalcogenide complexes, $Eu[H_3B{\cdot}EPh\text{-}\kappa E,H,H]_2(DME)_2$ (E = S for **1** and Se for **2**; DME = 1,2-Dimethoxyethane) and $Eu[EPh]_2$(18-C-6) (E = S for **3**, Se for **4**, and Te for **5**; 18-C-6 = 1,4,7,10,13,16-Hexaoxacyclooctadecane), were synthesized via reduction of diphenyl disulfide chalcogenide analogs with $Eu(BH_4)_2(THF)_2$ or NaH. The structures of these complexes were investigated by single-crystal X-ray diffraction, and their properties were characterized by thermogravimetric analysis and photophysical property tests. Complexes **1** and **2** are isomorphous and show similar yellowish-green luminescence, while complexes **3**–**5** have similar structures but crystallize in different space groups with bluish-green luminescence. This research reveals the influence of chalcogenide ligands on the 5d → 4f emission of Eu(II) complexes, providing a theoretical basis and new research ideas for the application of Eu(II) complexes in various fields, including luminescent materials, cryogenic refrigerants, and magnetic materials.

**Keywords:** divalent europium complexes; lanthanide chalcogenide complexes; luminescence; ligand field



Academic Editors: Debbie C. Crans and David Morales-Morales

Received: 19 November 2025
Revised: 9 December 2025
Accepted: 16 December 2025
Published: 17 December 2025

**Citation:** Wu, Z.-F.; Yang, Q.-S.; Ding, Y.-S.; Zheng, Z. Divalent Europium Complexes with Phenochalcogenato Ligands: Syntheses, Crystal Structures, and Luminescence Properties. *Inorganics* **2025**, *13*, 413. https://doi.org/10.3390/inorganics13120413



## 1. Introduction

The chemistry and materials of the lanthanide elements are dominated by their trivalent ions [1]. However, lanthanide ions in other oxidation states, namely +2, +4, and +5, have garnered growing interest as substances containing such ions display fascinating physicochemical properties that are starkly different from their trivalent counterparts [2–5]. Despite the generally difficult access to these ions inherent to their unique electronic structures, past decades have witnessed significant progress in the chemistry of lanthanide ions in unconventional oxidation states, most conspicuously for the divalent ions, but to a much lesser extent for the non-Ce tetravalent ions and even more limited for the exotic pentavalent species. By 2013, divalent complexes featuring all lanthanide elements but the radioactive promethium have been obtained and structurally characterized [6]. Among this group of lanthanide ions, Eu(II), together with Yb(II), is arguably the most studied one due

to its stability in aqueous solution and, more fundamentally, to its half-filled $4f^7$ electron configuration [2–5]. On the one hand, its large ground-state spin value makes it particularly valuable in the design of single-molecule magnets and other magnetic materials [7–12]. On the other hand, the Eu(II) ion features an excited-state configuration of $4f^65d^1$; the accessible $4f^65d^1 \rightarrow 4f^7$ transition gives a broad-band emission that is sensitively influenced by the ligand field as a result of the involvement of the d orbitals [13–15], which is distinctly different from the sharp red emission characteristic of the Eu(III) ion. A corollary is that the emission color of Eu(II)-containing species can be tuned by varying the ligand environment. Indeed, emissions spanning the entire ultraviolet and visible range have been observed using different ligands. This ligand-dependent luminescence trait of Eu(II) complexes makes them excellent materials for use as scintillators in medical imaging [16–18], phosphors in display technologies [19–27], and luminescence-based sensors for detecting pressure and temperature changes [28–30]. We note that a preponderance of Eu(II) complexes reported are with ligands featuring O as the coordinating atom [19–30]. Considering the enhanced softness of Eu(II) over Eu(III), it is fundamentally interesting to explore its coordination with heavier chalcogen-based ligands. On the one hand, this soft-soft match yields more stable complexes, enabling the isolation of unique molecular structures that are not accessible with oxides, resulting in novel coordination geometries and bonding scenarios that enrich and expand our fundamental understanding of lanthanide coordination chemistry. On the other hand, the heavier chalcogenides are strong-field ligands that cause a large crystal field splitting. A larger crystal field splitting lowers the energy of the emissive $4f^65d^1$ state, resulting in a systematic redshift of the emission [31]. By choosing sulfur (e.g., thiolates, thiophosphinates), selenium (selenolates), or tellurium (tellurolates) ligands, researchers can fine-tune the emission color in a predictable way. However, to the best of our knowledge, only a few Eu(II) complexes coordinated with S [32–43], Se [39,41,44–48], and Te [49–52] have been reported to date, and many of these serve as precursors for nanoparticles [33–35,39,41,46]. As a result, the understanding of the heavy-atom effect on the $5d \rightarrow 4f$ emission of Eu(II) complexes remains quite limited [31].

Recently, we reported that tuning the coordinated chalcogenide ligands can modulate the band gaps, magnetic anisotropy, and magnetic exchange couplings of trivalent lanthanide chalcogenide complexes [53–56]. In this work, we report five mononuclear Eu(II)-chalcogenide complexes, $Eu[H_3B{\cdot}EPh\text{-}\kappa E,H,H]_2(DME)_2$ (E = S for **1** and Se for **2**; DME = 1,2-Dimethoxyethane) and $Eu[EPh]_2$(18-C-6) (E = S for **3**, Se for **4**, and Te for **5**; 18-C-6 = 1,4,7,10,13,16-Hexaoxacyclooctadecane) and our initial efforts in exploring the ligand effects on the luminescence properties of these rare lanthanide complexes.

## 2. Results

### *2.1. Synthesis*

The reduction method is highly efficient for the synthesis of lanthanide chalcogenide complexes, where chalcogenide ligands are derived from elemental chalcogens or dichalcogenide complexes (REER, E = S, Se, or Te) [56,57]. To synthesize complexes **1**–**5**, chalcogenide analogs of diphenyl disulfide (PhEEPh, E = S, Se, or Te) were reduced using $Eu(BH_4)_2(THF)_2$ or NaH (Scheme 1). In the synthesis of **1** and **2**, PhEEPh (E = S or Se) underwent reduction by $BH_4^-$, generating $PhE^-$, $BH_3$, and $H_2$. As a soft Lewis acid, $BH_3$ readily binds to the soft Lewis base $PhE^-$ to form $H_3B{\cdot}EPh^-$. A similar phenomenon has recently been reported in the synthesis of U(III) chalcogenide complexes [58]. For complexes **3**–**5**, NaH simultaneously reduces Eu(III) to Eu(II) and PhEEPh (E = S, Se, or Te) to $PhE^-$ (E = S, Se, or Te). To satisfy the high coordination demand of the Eu(II) ion, 18-C-6 was introduced to facilitate the stabilization and crystallization of **3**–**5**. The 18-C-6

macrocycle encapsulates the Eu(II) ion at its center and coordinates to the equatorial plane of the Eu(II) ion [26,42,43,59–63].

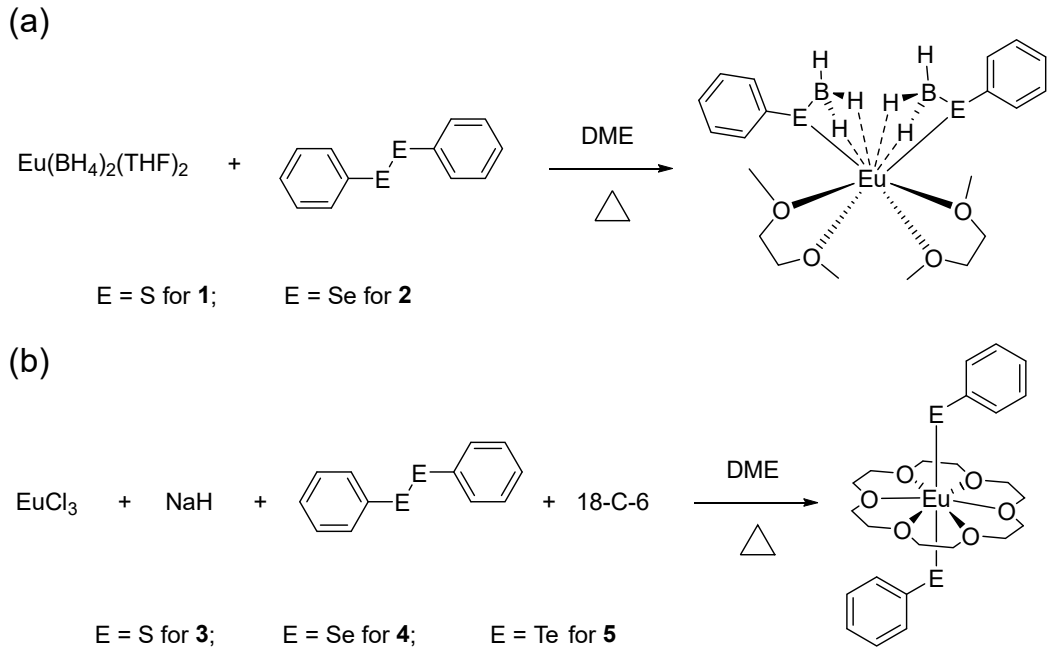


**Scheme 1.** The synthesis of complexes **1**–**2** (**a**) and **3**–**5** (**b**).

### *2.2. Crystal Structures*

As illustrated in Scheme 1, complexes **1**–**5** can be categorized into two groups: Eu[$H_3$B·EPh-κ*E*,*H*,*H*]$_2$(DME)$_2$ (E = S for **1** and Se for **2**) and Eu[EPh]$_2$(18-C-6) (E = S for **3**, Se for **4**, and Te for **5**). Single-crystal X-ray diffraction analysis (Table 1) confirmed that complexes **1** and **2** are isostructural, crystallizing in the monoclinic *C*2/c space group.

**Table 1.** Selected bond lengths (Å) and angles (°) for the complexes **1**–**5**.

| Identification Code | 1 | 2 | 3 | 4 | 5 |
|---|---|---|---|---|---|
| Empirical formula | $C_{20}H_{36}B_2EuO_4S_2$ | $C_{20}H_{36}B_2EuO_4Se_2$ | $C_{24}H_{34}EuO_6S_2$ | $C_{24}H_{34}EuO_6S_2$ | $C_{24}H_{34}EuO_6Te_2$ |
| Formula weight | 578.19 | 671.99 | 634.59 | 728.39 | 825.67 |
| Temperature/K | 100 | 100 | 100.03 | 100 | 100.00 |
| Crystal system | monoclinic | monoclinic | monoclinic | orthorhombic | orthorhombic |
| Space group | *C*2/c | *C*2/c | $P2_1/c$ | $Pna2_1$ | $Pna2_1$ |
| *a*/Å | 23.5147(7) | 23.6819(9) | 10.2493(3) | 25.6348(7) | 26.0466(7) |
| *b*/Å | 8.2207(3) | 8.3484(3) | 17.0490(6) | 8.7538(2) | 8.8152(2) |
| *c*/Å | 17.0919(9) | 17.1792(7) | 7.9684(2) | 11.7448(3) | 12.1672(3) |
| *α*/° | 90 | 90 | 90 | 90 | 90 |
| *β*/° | 130.4380(10) | 130.3130(10) | 112.0540(10) | 90 | 90 |
| *γ*/° | 90 | 90 | 90 | 90 | 90 |
| Volume/Å$^3$ | 2514.69(18) | 2589.85(17) | 1290.52(7) | 2635.56(12) | 2793.66(12) |
| 2Θ range for data collection/° | 5.45 to 55.01 | 5.43 to 54.98 | 4.91 to 55.04 | 4.92 to 55.13 | 5.71 to 55.01 |
| Reflections collected | 16,350 | 17,017 | 11,479 | 33,193 | 73,313 |
| Independent reflections | 2877 [$R_{int}$ = 0.0266, $R_{sigma}$ = 0.0193] | 2913 [$R_{int}$ = 0.0330, $R_{sigma}$ = 0.0231] | 2961 [$R_{int}$ = 0.0260, $R_{sigma}$ = 0.0238] | 6039 [$R_{int}$ = 0.0288, $R_{sigma}$ = 0.0255] | 6429 [$R_{int}$ = 0.0449, $R_{sigma}$ = 0.0248] |
| Data/restraints/parameters | 2877/0/145 | 2913/0/146 | 2961/0/151 | 6039/1/299 | 6429/1/298 |
| Goodness-of-fit on $F^2$ | 1.083 | 1.126 | 1.045 | 1.045 | 1.094 |
| Final *R* indexes [$I \geq 2\sigma$ ($I$)] | $R_1$ = 0.0130 $wR_2$ = 0.0330 | $R_1$ = 0.0161 $wR_2$ = 0.0388 | $R_1$ = 0.0159 $wR_2$ = 0.0369 | $R_1$ = 0.0130 $wR_2$ = 0.0286 | $R_1$ = 0.0182 $wR_2$ = 0.0416 |
| Final *R* indexes [all data] | $R_1$ = 0.0133 $wR_2$ = 0.0333 | $R_1$ = 0.0164 $wR_2$ = 0.0390 | $R_1$ = 0.0185 $wR_2$ = 0.0384 | $R_1$ = 0.0144 $wR_2$ = 0.0292 | $R_1$ = 0.0209 $wR_2$ = 0.0425 |

As depicted in Figure 1, the Eu(II) center in complexes **1** and **2** is coordinated by two DME molecules and two $H_3B{\cdot}EPh^-$ anions (E = S for **1** and Se for **2**). Each DME molecule binds to Eu(II) via a bidentate chelating mode through its two oxygen atoms, while the $H_3B{\cdot}EPh^-$ anions adopt a tridentate coordination mode—linking to the Eu(II) center via the chalcogen (E) atom and two hydrogen atoms from the $BH_3$ moiety. The average Eu-O bond lengths (Table 2) are 2.5796(10) Å for **1** and 2.5818(12) Å for **2**, which are consistent with the typical range reported for analogous Eu(II) complexes [19,21,26,42,43,59–63]. The Eu-E bond lengths are 3.0407(3) Å (E = S) for **1** and 3.1445(2) Å (E = Se) for **2**. These values are slightly longer than those of reported Eu-ER complexes [32–49], likely due to the formation of a Lewis acid-base adduct between the $BH_3$ (soft Lewis acid) and $PhE^-$ (soft Lewis base) moieties. This adduct formation modifies the ligand character, rendering them ether-like rather than phenochalcogenato ligands. The B-E bond length is 1.9486(16) Å (E = S) for **1** and 2.098(2) Å (E = Se) for **2**. The trend in B-E bond lengths—consistent with that of the Eu-E bond lengths—aligns with the increasing atomic radius of the chalcogen elements (S < Se) [64].

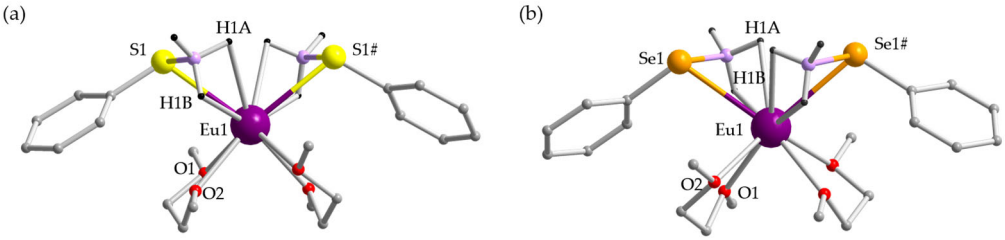


**Figure 1.** Ball-and-stick depiction of the crystal structures of **1** (**a**) and **2** (**b**). Colour legends: Eu, purple; O, red; C, gray; S, yellow; Se, Light orange; B, lavender; H, black. Other atoms are omitted for clarity. #: 1 − x, y, 0.5 − z.

**Table 2.** Selected bond lengths (Å) and angles (°) for the complexes **1** and **2**.

| **1** | | **2** | |
|---|---|---|---|
| Eu1-S1 | 3.0407(3) | Eu1-Se1 | 3.1445(2) |
| Eu1-O1 | 2.5716(10) | Eu1-O1 | 2.5799(12) |
| Eu1-O2 | 2.5875(10) | Eu1-O2 | 2.5837(12) |
| Eu1-H1A | 2.728(19) | Eu1-H1A | 2.55(2) |
| Eu1-H1B | 2.517(16) | Eu1-H1B | 2.71(2) |
| S1-B1 | 1.9486(16) | Se1-B1 | 2.098(2) |
| S1-Eu1-S1 $^{\#1}$ | 105.224(12) | Se1-Eu1-Se1 $^{\#1}$ | 103.744(7) |
| B1-Eu1-B1 $^{\#1}$ | 98.63(7) | B1-Eu1-B1 $^{\#1}$ | 99.20(8) |
| S1-Eu1-B1 | 38.22(3) | B1-Eu1-Se1 | 40.26(4) |
| O1-Eu1-O2 | 63.74(3) | O1-Eu1-O2 | 63.95(4) |

$^{\#1}$: 1 − x, y, 0.5 − z.

As illustrated in Table 1, complexes **3**–**5** exhibit analogous structural frameworks but differ in their crystal packing: complex **3** crystallizes in the monoclinic $P2_1/c$ space group, whereas complexes **4** and **5** adopt the orthorhombic $Pna2_1$ space group. Consistent with the coordination mode of reported Eu(II)-18-C-6 complexes [17,52–57], the 18-C-6 macrocycle in complexes **3**–**5** coordinates to the Eu(II) center at the equatorial plane, with two phenochalcogenato ($EPh^-$) ligands axially disposed on either side (Figure 2a–c). The Eu-O bond lengths in these complexes range from 2.6662(18) Å to 2.7343(11) Å (Table 2), which are consistent with the typical Eu-O bond lengths observed in other Eu(II)-18-C-6 adducts [26,42,43,59–62]. The Eu-S bond length in complex **3** is 2.9474(3) Å, shorter than that in complex **1** (3.0407(3) Å). This discrepancy arises from the different electronic states of the chalcogen atom: the S atom in **3** acts as an anionic phenochalcogenato ligand (electron-rich), whereas the S atom in **1** is part of the neutral $H_3B{\cdot}SPh^-$ adduct. Notably, complex **4**

(E = Se) and **5** (E = Te) exhibit distinct asymmetry in their axial Eu-E bond lengths: 3.0518(3) Å vs. 3.1180(3) Å for **4**, and 3.2585(3) Å vs. 3.3275(4) Å for **5**. This bond length disparity is tentatively attributed to differential intramolecular noncovalent interactions, as discussed in the following section. Across complexes **3**–**5**, the Eu-E bond lengths increase sequentially with the increasing atomic radius of the chalcogen elements (S < Se < Te) [64], adhering to the general trend of lanthanide-chalcogen bond length variation. The E-Eu-E bond angles are 180°, 172°, and 171° for **3**, **4**, and **5**, respectively, reflecting a near-linear axial coordination geometry. Additionally, the minimum equatorial O-Eu-O bond angles in all three complexes are close to 60°, confirming that the six oxygen atoms of 18-C-6 form a planar hexadentate coordination sphere around the Eu(II) center (Table 3).

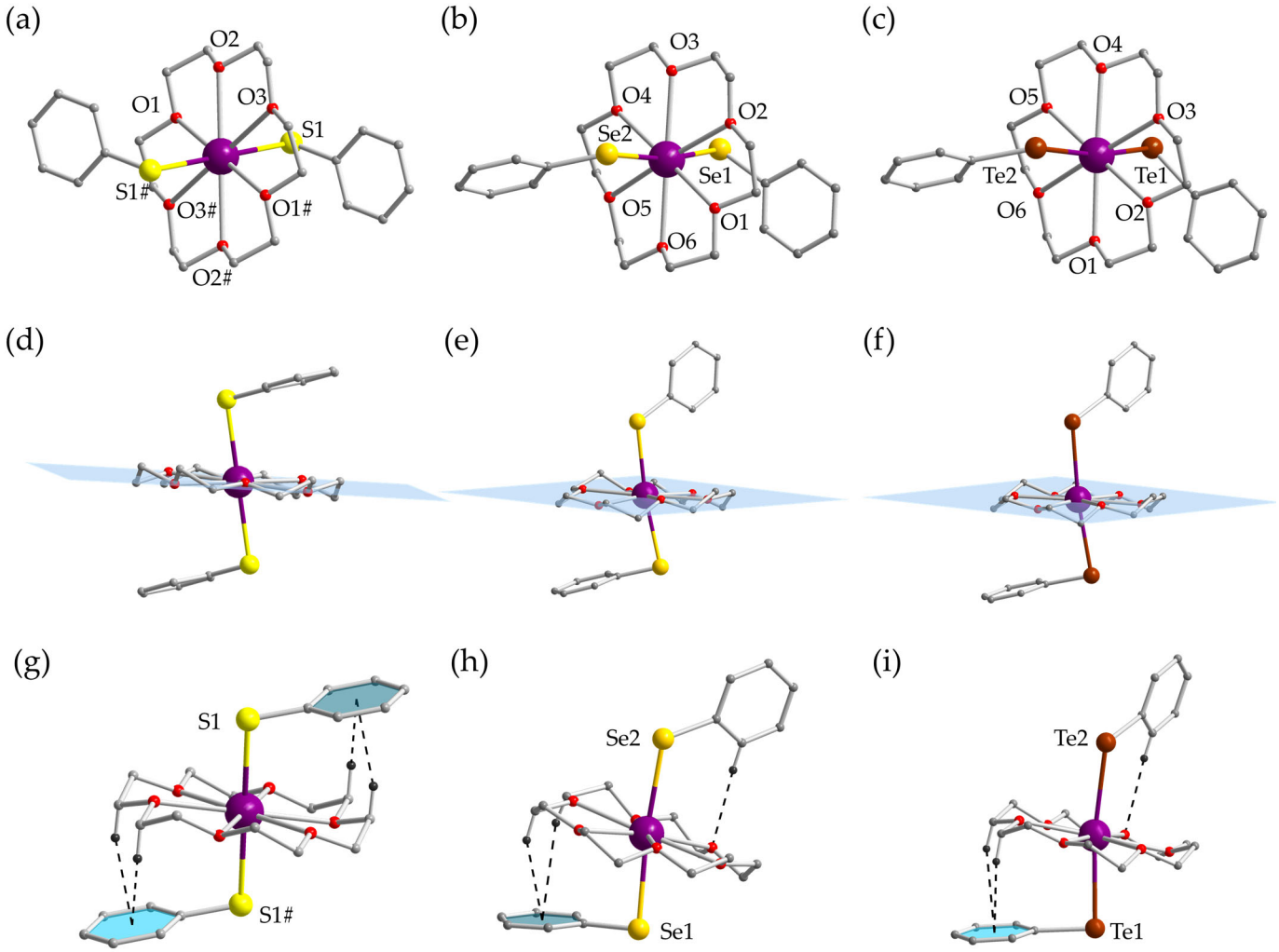


**Figure 2.** Ball-and-stick depiction of the crystal structures of **3** (**a**), **4** (**b**) and **5** (**c**), side view of **3** (**d**), **4** (**e**) and **5** (**f**) illustrating the tilt angles between the E-Eu-E axis and the 18-C-6 plane (blue plane), CH-π interactions and hydrogen bonds in **3** (**g**), **4** (**h**) and **5** (**i**). Colour legends: Eu, purple; O, red; C, gray; S, yellow; Se, Light orange; Te, brown; H, black. Other atoms are omitted for clarity. #: 1 − x, 1 − y, 1 − z.

In contrast to other reported Eu(II)-18-C-6 complexes [26,42,43,59–62], the E-Eu-E axis in complexes **3**–**5** is not perpendicular to the 18-C-6 equatorial plane. As summarized in Table 3, the E-Eu-O bond angles range from 79.18(3)° to 100.82(3)° for **3**, 74.92(4)° to 106.73(4)° for **4**, and 76.57(7)° to 102.40(7)° for **5**. This angular deviation results in tilt angles of 67.81°, 67.92°, and 70.08° between the E-Eu-E axis and the 18-C-6 plane for **3**, **4**, and **5**, respectively, (Figure 2d–f), indicating that the Eu(II) centers in these complexes adopt an

inclined hexagonal bipyramidal coordination geometry. Notably, distinct conformational differences were observed for the Ph substituents of the phenochalcogenato ligands: in complex **3**, the two Ph groups are nearly parallel to each other and approximately coplanar with the 18-C-6 plane. In contrast, complexes **4** and **5** exhibit asymmetric Ph group orientations—one Ph group is nearly parallel to the 18-C-6 plane, while the other is rotated by ~90° and nearly perpendicular to this plane. This conformational disparity correlates with different intramolecular noncovalent interactions: all Ph groups parallel to the 18-C-6 plane engage in strong CH-π interactions, where the 18-C-6 macrocycle acts as the CH donor and the Ph group serves as the π acceptor (Figure 2g–i). Conversely, Ph groups perpendicular to the 18-C-6 plane form hydrogen bonds with the macrocycle, with the Ph group functioning as the hydrogen bond donor and one oxygen atom of 18-C-6 as the acceptor (Figure 2h,i). A key structural correlation was identified: in complexes **4** (E = Se) and **5** (E = Te), the Eu-E bond length is significantly shorter when the adjacent Ph group participates in CH-π interactions (3.0518(3) Å for Eu-Se1 in **4** and 3.2585(3) Å for Eu-Te1 in **5**) compared to when it forms hydrogen bonds (3.1180(3) Å for Eu-Se2 in **4** and 3.3275(4) Å for Eu-Te2 in **5**). This observation suggests that CH-π interactions enhance the ligand field strength around the Eu(II) center. These ligand conformational differences and associated noncovalent interaction disparities are proposed to be the primary reason for the distinct space group assignments—monoclinic $P2_1/c$ for **3** vs. orthorhombic $Pna2_1$ for **4** and **5**—as noted earlier.

**Table 3.** Selected bond lengths (Å) and angles (°) for the complexes **3**–**5**.

| **3** | | **4** | | **5** | |
|---|---|---|---|---|---|
| Eu1-S1 | 2.9474(4) | Eu1-Se1 | 3.0518(3) | Eu1-Te1 | 3.2585(3) |
| - | - | Eu1-Se2 | 3.1180(3) | Eu1-Te2 | 3.3275(4) |
| Eu1-O1 | 2.7319(11) | Eu1-O1 | 2.7187(18) | Eu1-O1 | 2.695(3) |
| Eu1-O2 | 2.7343(11) | Eu1-O2 | 2.6662(18) | Eu1-O2 | 2.708(3) |
| Eu1-O3 | 2.7062(11) | Eu1-O3 | 2.7224(19) | Eu1-O3 | 2.667(3) |
| - | - | Eu1-O4 | 2.7098(19) | Eu1-O4 | 2.733(3) |
| - | - | Eu1-O5 | 2.7248(18) | Eu1-O5 | 2.711(3) |
| - | - | Eu1-O6 | 2.7092(19) | Eu1-O6 | 2.718(3) |
| *Avg*. [a] Eu-O | 2.72 | *Avg*. Eu-O | 2.71 | *Avg*. Eu-O | 2.71 |
| S1-Eu1-S1 [#1] | 180.0 | Se1-Eu1-Se2 | 170.536(9) | Te1-Eu1-Te2 | 171.536(10) |
| O1-Eu1-O2 | 60.91(3) | O1-Eu1-O2 | 59.33(6) | O1-Eu1-O2 | 60.03(10) |
| O2-Eu1-O3 | 60.28(3) | O2-Eu1-O3 | 61.54(6) | O2-Eu1-O3 | 59.46(10) |
| O3 [#1]-Eu1-O1 | 59.44(4) | O3-Eu1-O4 | 60.29(6) | O3-Eu1-O4 | 60.84(10) |
| - | - | O4-Eu1-O5 | 59.04(5) | O4-Eu1-O5 | 59.96(10) |
| - | - | O5-Eu1-O6 | 60.80(6) | O5-Eu1-O6 | 59.40(10) |
| - | - | O6-Eu1-O1 | 60.22(6) | O6-Eu1-O1 | 60.99(10) |
| *Avg*. [b] O-Eu-O | 60.21 | *Avg*. O-Eu-O | 60.20 | *Avg*. O-Eu-O | 60.11 |
| *Rng*. [c] S-Eu-O | 79.18(3)–100.82(3) | *Rng*. Se-Eu-O | 74.92(4)–106.73(4) | *Rng*. Te-Eu-O | 76.57(7)–102.40(7) |

[#1]: 1 − x, 1 − y, 1 − z. [a]: average Eu-O bond lengthes; [b]: average O-Eu-O angles; [c]: the rang of the S-Eu-O angles.

### *2.3. Thermogravimetric Analysis*

Many Eu(II) complexes have been reported as precursors for Eu(II) chalcogenide nanomaterials [33–35,39,41,46]. Thermogravimetric analysis (TGA, Figure 3) was performed to evaluate the thermal stability and identify the decomposition behavior of complexes **3**–**5**. All three complexes exhibit good thermal stability up to 150 °C, followed by a rapid mass loss in the temperature range of 200–350 °C. The decomposition reaches a plateau with residual mass relative to the initial mass of 26.10% at 700 °C for **3**, 23.28% at 850 °C for **4**, and 19.51% at 750 °C for **5**. The residue from the TGA analysis is assigned to EuO (*M*r. 167.96 g/mol) as the thermal decomposition was carried out under an argonn atmosphere; a good match between the above experimental results and the theoretical values, respectively, 26.47%, 23.06%, and 20.34% for **3**–**5**, is obtained. Such a result implies that the two $PhE^-$

ligands in complexes **3**–**5** decompose before the 18-C-6 macrocycle. Notably, the TGA curve of complex **5** reveals that the decomposition of 18-C-6 likely proceeds through three distinct stages.

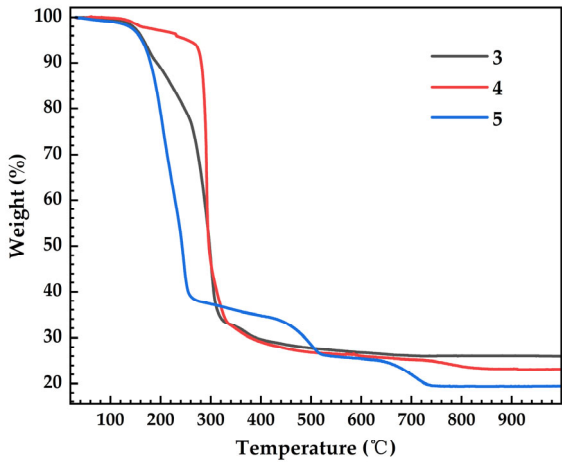


**Figure 3.** TGA curves of **3**–**5**.

### *2.4. Photophysical Properties*

To investigate the luminescent properties of the five complexes, emission spectra were collected in the solid powder state at different temperatures (Figures 4 and 5). The five complexes exhibit luminescent emission in the range of 400–750 nm, which is within the expected range for the 5d → 4f transition of the Eu(II) complexes [13–30].

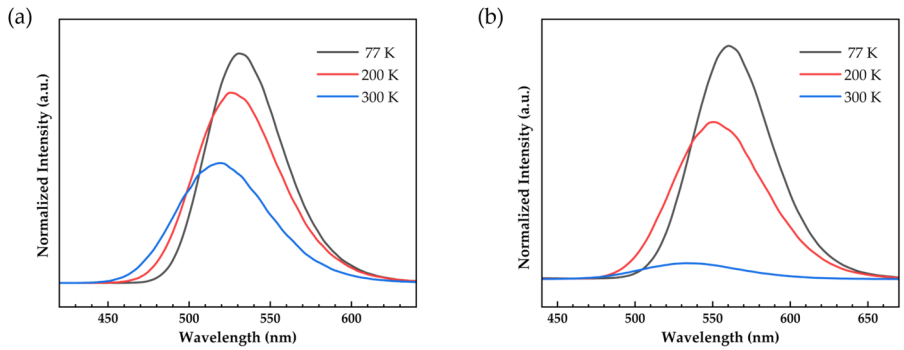


**Figure 4.** The emissions of solid-state **1** (**a**) and **2** (**b**) at the indicated temperatures.

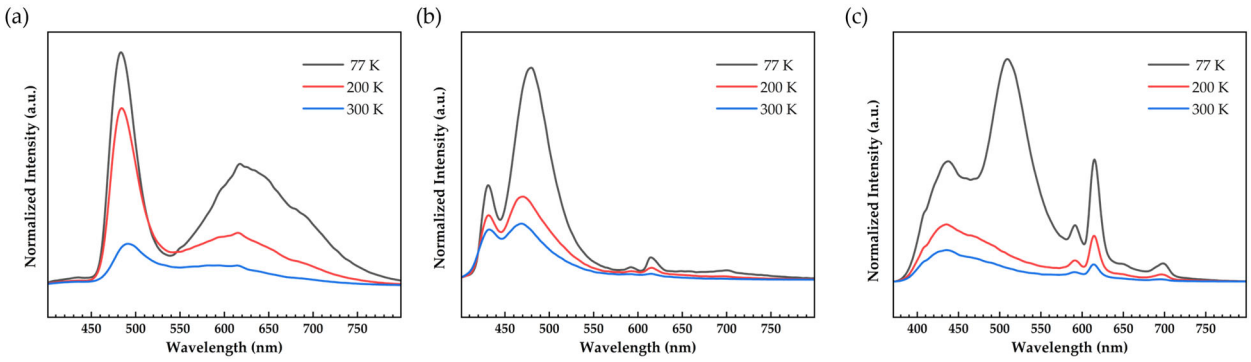


**Figure 5.** The emissions of solid-state **3** (**a**), **4** (**b**) and **5** (**c**) at the indicated temperatures.

At 300 K, complexes **1** and **2** exhibit single broad emissions (Figure 4) with maximum peaks at 519 nm and 537 nm, respectively. The redshift of the 5d → 4f transition from **1** to **2** is primarily attributed to the heavy atom effect—with S in **1** replaced by Se in **2**—which

lowers the energy level of the lowest 5d excited state. This phenomenon is consistent with the heavy atom effect on the 5d → 4f emission of Ce(III) complexes recently reported by Liu et al. [31]. For both complexes, a slight redshift and enhanced emission intensity are observed with decreasing temperature. Specifically, the emission maximum of **1** shifts to 530 nm at 200 K and 534 nm at 77 K, while that of **2** shifts to 551 nm at 200 K and 563 nm at 77 K. Additionally, the emission intensity increases by approximately 2-fold for **1** and ~15-fold for **2** when the temperature decreases from 300 K to 77 K. These results suggest that complexes **1** and **2** hold potential for applications in band-shift-based luminescence thermometers and/or ratiometric optical thermometers [28–30].

The luminescence emissions of complexes **3**–**5** are significantly broader in the 400–750 nm range (Figure 5) at 300 K, with up to five distinct peaks observed for complex 5 at 77 K (Figure 5c). This multi-peak emission is presumably derived from the splitting of the 5d orbital into five energy levels under the influence of the ligand field, which undergo radiative transitions to the $4f^7$ ground state. A similar phenomenon has been well-documented for Ce(III) complexes exhibiting 5d → 4f emissions [31]. It is widely recognized that the hexagonal bipyramidal coordination environment—featuring six equatorial oxygen atoms from 18-C-6 and two axial anionic ligands—typically generates a strong ligand field around lanthanide ions [65–67]. As described earlier, the Eu(II) centers in complexes **3**–**5** adopt this coordination geometry, with two phenochalcogenato ligands occupying the axial positions. The strong ligand field induced by these axial phenochalcogenato ligands is believed to be the primary driver for the splitting of the Eu(II) 5d orbital. In contrast, the ligand field around the Eu(II) ion in complexes **1** and **2** approximates spherical symmetry, leading to minimal splitting of the 5d levels [13–15,68,69]. Consequently, complexes **1** and **2** exhibit single, narrow-band emissions, in contrast to the broad, multi-peak emissions of complexes **3**–**5** (Figures 4–6). Consistent with this trend, spherical ligand fields are commonly utilized in the design of Eu(II)-based luminescent materials with narrow-band emission characteristics [16–18]. Conversely, Eu(II) complexes with axial ligand fields—such as **3**–**5**—hold promise as potential candidates for broad-emission organic light-emitting diodes (OLEDs) [20–25].

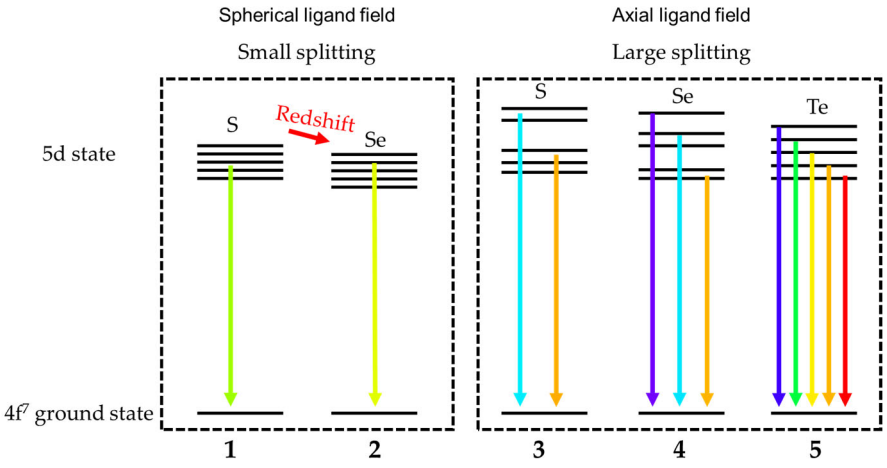


**Figure 6.** Schematic energy diagrams of the ligand-field splitting of the 5d orbitals and the emission spectra for **1**–**5**.

## 3. Materials and Methods

### *3.1. General Considerations*

All manipulations were conducted using standard Schlenk techniques or within a glovebox under an argon atmosphere. The glassware was dried overnight at 120 °C before use. Anhydrous $EuCl_3$ [70] and $Eu(BH_4)_2(THF)_2$ [19] were synthesized follow-

ing established procedures from the literature. All other reagents were procured from Energy-Chemical (Shanghai, China): anhydrous solvents, including THF (99.5%, Extra Dry, Water $\leq$ 30 ppm), DME (99%, Extra Dry, stabilized with BHT, Water $\leq$ 30 ppm), pyridine (99.5%, Extra Dry, Water $\leq$ 50 ppm) and n-hexane (99%, Extra Dry, with molecular sieves, Water $\leq$ 50 ppm) were stored with molecular sieves; NaH (60% dispersion in mineral oil) was washed with n-hexane to remove mineral oil to a fine powder and dried under vacuum before use; PhSSPh (98%), PhSeSePh (97%), PhTeTePh (96%), $NaBH_4$ (98%) and 18-C-6 (AR, $\geq$99.5%) were used without further purification. Elemental analyses for carbon (C) and hydrogen (H) were performed using a Thermo FLASH2000 elemental analyzer (Waltham, MA, USA).

### *3.2. Synthesis of Complexes **1**–**5***

Synthesis of Eu[$H_3B$·SPh-κ*S*,*H*,*H*]$_2$(DME)$_2$ (**1**): All manipulations were performed under an inert atmosphere using standard Schlenk techniques to prevent oxidation of Eu(II) species. A dry Schlenk flask was sequentially charged with Eu$(BH_4)_2(THF)_2$ (89 mg, 0.3 mmol), PhSSPh (65 mg, 0.3 mmol), and 10 mL of anhydrous DME. The reaction mixture was magnetically stirred until a homogeneous suspension was formed. At the initial reaction stage, slight effervescence was observed alongside the formation of a white precipitate—clear evidence for the initiation of redox reactions. The mixture was then heated to 80 °C and stirred at this temperature for 2 h, during which the suspension gradually turned yellow-green and most of the white precipitate dissolved. The remaining trace white precipitate was removed by filtration to afford a clear yellow-green filtrate. The filtrate was concentrated under reduced pressure to a volume of ~2 mL, and 10 mL of anhydrous n-hexane was carefully layered onto the concentrated solution. After standing undisturbed for 2 days, yellow-green needle-like crystals of **1** (suitable for single-crystal X-ray diffraction) were obtained at the solvent interface. The crystals were collected by filtration, washed with cold n-hexane (3 × 5 mL), and dried under high vacuum for 2 h to yield the target complex **1** as a yellow-green crystalline solid. Yield: 121 mg (70%, based on Eu$(BH_4)_2(THF)_2$. Anal. Calcd for $C_{20}H_{36}B_2EuO_4S_2$: C 41.51, H 6.23; Found: C 41.51, H 6.50.

Synthesis of Eu[$H_3B$·SePh-κ*Se*,*H*,*H*]$_2$(DME)$_2$ (**2**): The synthesis of complex 2 followed a protocol analogous to that of complex **1**, with the sole modification of substituting PhSSPh with PhSeSePh (94 mg, 0.3 mmol). After standing undisturbed for 2 days, yellow needle-like crystals of **2**—suitable for single-crystal X-ray diffraction analysis—were obtained at the solvent interface. The crystals were collected, washed, and dried under high vacuum to afford a yellow crystalline solid. Yield: 140 mg (70%, based on Eu$(BH_4)_2(THF)_2$). Anal. Calcd for $C_{20}H_{36}B_2EuO_4Se_2$: C 35.71, H 5.36; Found: C 36.20, H 4.94.

Synthesis of Eu[SPh]$_2$(18-C-6) (**3**): Under an inert atmosphere, a dry Schlenk flask was sequentially charged with EuCl3 (89 mg, 0.3 mmol), PhSSPh (65 mg, 0.3 mmol), 18-C-6 (79 mg, 0.3 mmol), NaH (22 mg, 0.9 mmol), and 10 mL of anhydrous DME. The mixture was vigorously stirred until a homogeneous white suspension was formed. The reaction mixture was then stirred at 80 °C overnight, during which the suspension color gradually transitioned from white to bright yellow, providing clear evidence for the reduction of Eu(III) to Eu(II). After cooling to room temperature, the colorless supernatant was removed by filtration, leaving a yellow precipitate. This precipitate was extracted with 10 mL of anhydrous pyridine, and the resulting yellow pyridine solution (obtained via filtration to remove insoluble residues) was layered with 10 mL of anhydrous n-hexane. After standing undisturbed for 2 days, yellow block-shaped crystals of **3** (suitable for single-crystal X-ray diffraction) were obtained. The crystals were collected by filtration, washed with a pyridine/n-hexane mixture (1:5, $v/v$, 3 × 5 mL), and dried under high vacuum for

2 h to afford the target complex **3** as a yellow crystalline solid. Yield: 125 mg (66%, based on $EuCl_3$). Anal. Calcd for $C_{24}H_{34}EuO_6S_2$: C 45.39, H 5.36; Found: C 46.89, H 5.25.

Synthesis of Eu[SePh]$_2$(18-C-6) (**4**): The synthesis of complex **4** followed a protocol analogous to that of complex **3**, with the sole modification of substituting PhSSPh with PhSeSePh (94 mg, 0.3 mmol). After standing undisturbed for 2 days, yellow needle-like crystals of **4**—suitable for single-crystal X-ray diffraction analysis—were obtained at the solvent interface. The crystals were collected, washed, and dried under high vacuum to afford a yellow crystalline solid. Yield: 131 mg (60%, based on $EuCl_3$). Anal. Calcd for $C_{24}H_{34}EuO_6Se_2$: C 39.54, H 4.67; Found: C 39.61, H 4.69.

Synthesis of Eu[TePh]$_2$(18-C-6) (**5**): The synthesis of complex **5** followed a protocol analogous to that of complex **3**, with the sole modification of substituting PhSSPh with PhTeTePh (123 mg, 0.3 mmol). After standing undisturbed for 2 days, yellow needle-like crystals of **5**—suitable for single-crystal X-ray diffraction analysis—were obtained at the solvent interface. The crystals were collected, washed, and dried under high vacuum to afford a yellow crystalline solid. Yield: 64 mg (26%, based on $EuCl_3$). Anal. Calcd for $C_{24}H_{34}EuO_6Te_2$: C 34.88, H 4.12; Found: C 35.01, H 4.32.

### *3.3. Crystal Structure Determination*

Single-crystal X-ray diffraction (SXRD) studies were conducted using Bruker D8 Venture (Mo *Kα* radiation (λ = 0.71073 Å)) (Bruker, Berlin, Germany) at 100 K for **1**–**5**. Using Olex2 (v1.5), the structure was solved with the SHELXT structure solution program, employing intrinsic phasing, and refined with the SHELXL refinement package using least-squares minimization [71–73]. All hydrogen atoms were placed in calculated, ideal positions and refined as riding on their respective carbon atoms, with displacement parameters also dependent on the parent carbon atom $U_{eq}$ value.

### *3.4. Thermogravimetric Analysis*

The TGA analyses were performed on a Mettler Toledo TGA-2 thermal gravimetric analyzer (METTLER TOLEDO, Greifensee, Switzerland) with a heating rate of 10 °C/min under an argon atmosphere. The sample masses used for TGA are 4.1360 mg for **1**, 1.6070 mg for **2**, 3.2870 mg for **3**, 2.5560 mg for **4**, and 2.6090 mg for **5**. The weight losses were measured from room temperature up to 1000 °C.

### *3.5. Photophysical Characterization*

Excitation (Figure S1) and emission spectra were collected using a steady-state spectrometer (FLS-1000) (Edinburgh Instruments, Edinburgh, UK) with a xenon lamp. Solid samples of the measured complexes were ground and pressed between two quartz microscope slides, sealed with wax to prevent sample oxidation during both room-temperature and low-temperature measurements. Low-temperature emission spectra were collected using an Oxford Optistat DN liquid nitrogen cryostat (Oxford Instruments, Oxford, UK).

## 4. Conclusions

In this study, five mononuclear Eu(II)-chalcogenide complexes were successfully synthesized, and their crystal structures and physicochemical properties were comprehensively characterized. Single-crystal X-ray diffraction analysis elucidated the structural features of these complexes, which can be classified into two distinct groups: complexes **1** and **2** are isostructural, while complexes **3**–**5** share analogous structural frameworks but crystallize in different space groups. Thermogravimetric analysis revealed that complexes **3**–**5** exhibit good thermal stability below 150 °C. The decomposition processes reach a plateau, with residual masses of ~26.1% (700 °C), 23.3% (850 °C), and 19.5% (750 °C) for **3**,

**4**, and **5**, respectively—tentatively assigned to EuO based on the theoretical mass fraction of Eu-containing residues. Photophysical property measurements demonstrated that under 365 nm excitation, Complexes **1** and **2** emit intense yellowish-green luminescence, whereas complexes **3**–**5** exhibit bluish-green emission. These results confirm the significant regulatory effect of chalcogenide ligands on the 5d → 4f emission behavior of Eu(II) complexes, along with distinct structural and photophysical differences between the two groups of complexes. Future research could further expand the library of Eu(II)-chalcogenide complexes by exploring diverse chalcogenide ligands and systematically investigating their structure-property relationships to broaden their applications in luminescent materials, cryogenic refrigeration, magnetic materials, luminescent thermometers, and X-ray detection/imaging. By optimizing ligand architectures and coordination environments, the development of high-performance Eu(II) complex-based materials is anticipated, which may provide innovative solutions to critical challenges in practical applications and thereby advance the sustainable development of these fields.

**Supplementary Materials:** The following supporting information can be downloaded at: https://www.mdpi.com/article/10.3390/inorganics13120413/s1. Table S1: Selected bond distances (Å) and angles (°) for **1**; Table S2: Selected bond distances (Å) and angles (°) for **2**; Table S3: Selected bond distances (Å) and angles (°) for **3**; Table S4: Selected bond distances (Å) and angles (°) for **4**; Table S5: Selected bond distances (Å) and angles (°) for **5**; Figure S1: Excitation spectra of solid-state **1**–**5** at room temperature.

**Author Contributions:** Conceptualization, Z.Z. and Y.-S.D.; methodology, Z.-F.W.; investigation, Z.-F.W.; data curation, Y.-S.D., Z.-F.W. and Q.-S.Y.; writing—original draft preparation, Y.-S.D. and Z.-F.W.; writing—review and editing, Z.Z. and Y.-S.D.; supervision, Z.Z. and Y.-S.D.; project administration, Z.Z. and Y.-S.D.; funding acquisition, Z.Z. and Y.-S.D. All authors have read and agreed to the published version of the manuscript.

**Funding:** This work was supported by the National Natural Science Foundation of China (92261203, 22101116, and 21971106), Key Laboratory of Rare-Earth Chemistry of Guangdong Higher Education Institutes (2022KSYS006), and Shenzhen Fundamental Research Program (JCYJ20220530115001002 and JCYJ20220818100417037).

**Institutional Review Board Statement:** Not applicable.

**Informed Consent Statement:** Not applicable.

**Data Availability Statement:** Crystal data, details of the data collection and refinement are given in Table 1. Selected bond distances (Å) and angles (°) are given in Tables S1–S5. Crystallographic data for the structures have been deposited with the Cambridge Crystallographic Data Centre (2501107 (**1**), 2501108 (**2**), 2501109 (**3**), 2501110 (**4**), and 2501111 (**5**)). Copies of this information may be obtained free of charge from The Director, CCDC, 12 Union Road, Cambridge, CB2 1EZ, UK (fax: +44-1223-336033; email: deposit@ccdc.cam.ac.uk or https://www.ccdc.cam.ac.uk (accessed on 7 November 2025)). Other data are contained within the article and Supplementary Materials.

**Conflicts of Interest:** The authors declare no conflicts of interest.

## References

1. Huang, C. *Rare Earth Coordination Chemistry: Fundamentals and Applications*; John Wiley & Sons: Hoboken, NJ, USA, 2010. [CrossRef]
2. Wang, Y.; Huang, W. Chemistry of Non-Traditional Oxidation States of Rare Earth Metals. *Sci. Sin. Chim.* **2020**, *50*, 1504–1559. [CrossRef]
3. Wedal, J.C.; Evans, W.J. A Rare-Earth Metal Retrospective to Stimulate All Fields. *J. Am. Chem. Soc.* **2021**, *143*, 18354–18367. [CrossRef] [PubMed]
4. Ye, L.-W.; Hu, H.-S.; Schwarz, W.H.E.; Li, J. Physical Origin and Periodicity of the Highest Oxidation States in Heavy-Element Chemistry. *Acc. Chem. Res.* **2025**, *58*, 1903–1912. [CrossRef]

5. Ding, Y.-S.; Yang, Q.-S.; Zheng, Z. Pentavalent Praseodymium Complexes Culminated in the Pursuit of High-valence Lanthanide Compounds. *Chin. J. Struct. Chem.* **2025**, *44*, 100696. [CrossRef]
6. MacDonald, M.R.; Bates, J.E.; Ziller, J.W.; Furche, F.; Evans, W.J. Completing the Series of +2 Ions for the Lanthanide Elements: Synthesis of Molecular Complexes of $Pr^{2+}$, $Gd^{2+}$, $Tb^{2+}$, and $Lu^{2+}$. *J. Am. Chem. Soc.* **2013**, *135*, 9857–9868. [CrossRef]
7. Wang, Y.; Xiang, J.; Zhang, L.; Gong, J.; Li, W.; Mo, Z.; Shen, J. Giant Low-Field Cryogenic Magnetocaloric Effect in a Polycrystalline $EuB_4O_7$ Compound. *J. Am. Chem. Soc.* **2024**, *146*, 3315–3322. [CrossRef]
8. Wang, B.; Liu, X.; Hu, F.; Wang, J.-T.; Xiang, J.; Sun, P.; Wang, J.; Sun, J.; Zhao, T.; Mo, Z.; et al. A Record-High Cryogenic Magnetocaloric Effect Discovered in $EuCl_2$ Compound. *J. Am. Chem. Soc.* **2024**, *146*, 35016–35022. [CrossRef]
9. Mo, Z.; Jiang, J.; Tian, L.; Xie, H.; Li, Y.; Zheng, X.; Zhang, L.; Gao, X.; Li, Z.; Liu, G.; et al. Ferromagnetic $Eu_2SiO_4$ Compound with a Record Low-Field Magnetocaloric Effect and Excellent Thermal Conductivity Near Liquid Helium Temperature. *J. Am. Chem. Soc.* **2025**, *147*, 14684–14693. [CrossRef]
10. Chen, H.; Manvell, A.S.; Kubus, M.; Dunstan, M.A.; Lorusso, G.; Gracia, D.; Jørgensen, M.S.B.; Kegnæs, S.; Wilhelm, F.; Rogalev, A.; et al. Towards Frustration in Eu(II) Archimedean tessellations. *Chem. Commun.* **2023**, *59*, 1609–1612. [CrossRef]
11. Manvell, A.S.; Dunstan, M.A.; Gracia, D.; Hrubý, J.; Kubus, M.; McPherson, J.N.; Palacios, E.; Weihe, H.; Hill, S.; Schnack, J.; et al. A Triangular Frustrated Eu(II)–Organic Framework for Sub-Kelvin Magnetic Refrigeration. *J. Am. Chem. Soc.* **2025**, *147*, 7597–7603. [CrossRef] [PubMed]
12. Errulat, D.; Harriman, K.L.M.; Gálico, D.A.; Salerno, E.V.; van Tol, J.; Mansikkamäki, A.; Rouzières, M.; Hill, S.; Clérac, R.; Murugesu, M. Slow Magnetic Relaxation in a Europium(II) Complex. *Nat. Commun.* **2024**, *15*, 3010. [CrossRef]
13. Wang, L.; Fang, P.; Zhao, Z.; Huang, Y.; Liu, Z.; Bian, Z. Rare Earth Complexes with 5d–4f Transition: New Emitters in Organic Light-Emitting Diodes. *J. Phys. Chem. Lett.* **2022**, *13*, 2686–2694. [CrossRef] [PubMed]
14. Li, J.; Zhao, Y.; Yu, D.; Zhan, C. Recent Advances in d-f Transition Lanthanide Complexes for Organic Light-Emitting Diodes: Insights Into Structure–Luminescence Relationships. *Laser Photonics Rev.* **2025**, *19*, 2402198. [CrossRef]
15. Liu, Y.; Ganesan, P.; Gao, P. Harnessing d-f transition rare earth complexes for single layer white organic light emitting diodes. *Chin. J. Struct. Chem.* **2024**, *43*, 100369. [CrossRef]
16. Han, K.; Jin, J.; Wang, Y.; Zhou, X.; Sun, Y.; Chen, L.; Xia, Z. Hybrid Eu(II)-Bromide Scintillators with Efficient 5d-4f Bandgap Transition for X-ray Imaging. *Light Sci. Appl.* **2024**, *13*, 222. [CrossRef]
17. Li, L.; Wang, Y.; Jin, J.; Han, K.; Zhang, S.; Xia, Z. Organic Cation Methylation Design of Hybrid Eu(II)-based Halide Scintillators for Improved X-Ray Detection and Imaging. *Adv. Mater.* **2025**, e10379. [CrossRef]
18. Chen, L.; Zhang, S.; Wang, Y.; Li, L.; Chen, D.; Han, K.; Xia, Z. Suppressed Concentration Quenching via Divalent Eu/Sr Alloying in Hybrid Iodides Scintillators Toward Bright Luminescence for X-ray Imaging. *Angew. Chem. Int. Ed.* **2025**, *64*, e202514331. [CrossRef]
19. Marks, S.; Heck, J.G.; Habicht, M.H.; Oña-Burgos, P.; Feldmann, C.; Roesky, P.W. $[Ln(BH_4)_2(THF)_2]$ (Ln = Eu, Yb)—A Highly Luminescent Material. Synthesis, Properties, Reactivity, and NMR Studies. *J. Am. Chem. Soc.* **2012**, *134*, 16983–16986. [CrossRef]
20. Li, J.; Wang, L.; Zhao, Z.; Sun, B.; Zhan, G.; Liu, H.; Bian, Z.; Liu, Z. Highly Efficient and Air-Stable Eu(II)-Containing Azacryptates Ready for Organic Light-Emitting Diodes. *Nat. Commun.* **2020**, *11*, 5218. [CrossRef]
21. Yan, W.; Li, T.; Cai, Z.; Qi, H.; Guo, R.; Huo, P.; Liu, Z.; Bian, Z. Systematic Tuning of the Emission Colors and Redox Potential of Eu(II)-Containing Cryptates by Changing the N/O Ratio of Cryptands. *Inorg. Chem. Front.* **2022**, *9*, 4794–4800. [CrossRef]
22. Wu, A.; Huo, P.; Yu, G.; Guo, R.; Zhao, Z.; Yan, W.; Wang, L.; Bian, Z.; Liu, Z. Europium(II) Complexes with Substituted Tris(2-aminoethyl)amine/Triethanolamine Ligand and their Application in Blue Spin-Coated Organic Light-Emitting Diodes. *Adv. Opt. Mater.* **2022**, *10*, 2200952. [CrossRef]
23. Hay, M.A.; Gable, R.W.; Boskovic, C. Modulating the Electronic Properties of Divalent Lanthanoid Complexes with Subtle Ligand Tuning. *Dalton Trans.* **2023**, *52*, 3315–3324. [CrossRef] [PubMed]
24. Yan, W.; Li, Y.; Huo, P.; Guo, R.; Yu, G.; Zhao, Z.; Wang, K.; Bian, Z.; Liu, Z. Fine Tuning the Steric Hindrance of the Eu(II) Tris(pyrazolyl)borate Complex for a Blue Organic Light-Emitting Diode. *J. Mater. Chem. C* **2024**, *12*, 9834–9840. [CrossRef]
25. Bai, R.; Huo, P.; Zheng, N.; Li, Y.; Yan, W.; Fang, P.; Zhou, X.; Bian, Z.; Liu, Z. Europium(II) Complex with d-f Transition: New Emitter for Blue Light-Emitting Electrochemical Cells with an External Quantum Efficiency of 19.8%. *Adv. Mater.* **2025**, *37*, 2419849. [CrossRef]
26. Bonnin, M.A.; Leicht, S.; Feldmann, C. Crown-Ether Coordination Compounds of Europium and 24-Crown-8. *Inorg. Chem.* **2025**, *64*, 723–730. [CrossRef]
27. Li, L.; Jin, J.; Han, K.; Wang, Y.; Xia, Z. Rational Design and Synthesis of Narrow-Band Emitting Eu(II)-Based Hybrid Halides via Alkyl Thermal Cleavage. *Nat. Commun.* **2025**, *16*, 7479. [CrossRef]
28. Diaz-Rodriguez, R.M.; Gálico, D.A.; Chartrand, D.; Suturina, E.A.; Murugesu, M. Toward Opto-Structural Correlation to Investigate Luminescence Thermometry in an Organometallic Eu(II) Complex. *J. Am. Chem. Soc.* **2022**, *144*, 912–921. [CrossRef]
29. Diaz-Rodriguez, R.M.; Gálico, D.A.; Chartrand, D.; Murugesu, M. Ligand Effects on the Emission Characteristics of Molecular Eu(II) Luminescence Thermometers. *J. Am. Chem. Soc.* **2024**, *146*, 34118–34129. [CrossRef] [PubMed]

30. Diaz-Rodriguez, R.M.; Gálico, D.A.; Murugesu, M. Exploring a New Family of (Phosphinochalcogenoyl)Europocenes for Magneto-Optical Thermometry. *Angew. Chem. Int. Ed.* **2025**, *64*, e202517812. [CrossRef]
31. Zheng, J.; Li, Z.; Guo, R.; Qi, H.; Liu, H.; Li, Y.; Niu, H.; Jiang, H.; Bian, Z.; Liu, Z. Heavy-Atom-Induced Narrow Emission in Chalcogen-Coordinating Lanthanide Cerium(III) Complexes. *Aggregate* **2025**, *6*, e70015. [CrossRef]
32. Mashima, K.; Nakayama, Y.; Fukumoto, H.; Kanehisa, N.; Kai, Y.; Nakamura, A. Formation of Lanthanoid(II) and Lanthanoid(III) Thiolate Complexes Derived from Metals and Organic Disulfides: Crystal Structures of [{Ln(SAr)(μ-SAr)(thf)$_3$}$_2$](Ln = Sm, Eu), [Sm(SAr)$_3$(py)$_2$(thf)] and [Yb(SAr)$_3$(py)$_3$](Ar = 2,4,6-triisopropylphenyl; py = pyridine). *J. Chem. Soc. Chem. Commun.* **1994**, 2523–2524. [CrossRef]
33. Brewer, M.; Lee, J.; Brennan, J.G. Heterometallic Eu/M(II) Benzenethiolates (M = Zn, Cd, Hg): Synthesis, Structure, and Thermolysis Chemistry. *Inorg. Chem.* **1995**, *34*, 5919–5924. [CrossRef]
34. Berardini, M.; Brennan, J. Europium Pyridinethiolates: Synthesis, Structure, and Thermolysis. *Inorg. Chem.* **1995**, *34*, 6179–6185. [CrossRef]
35. Melman, J.H.; Emge, T.J.; Brennan, J.G. Fluorinated Thiolates of Divalent and Trivalent Lanthanides. Ln−F Bonds and the Synthesis of $LnF_3$. *Inorg. Chem.* **2001**, *40*, 1078–1081. [CrossRef]
36. Angelkort, J.; van Smaalen, S.; Hauber, S.O.; Niemeyer, M. Phase Transition and Crystal Structure of the Monomeric Europium(II) Thiolate Eu(SC$_{36}$H$_{49}$)$_2$. *Z. Anorg. Allg. Chem.* **2007**, *633*, 1031–1035. [CrossRef]
37. Bakker, J.M.; Deacon, G.B.; Forsyth, C.M.; Junk, P.C.; Wiecko, M. A Structural Investigation of Trivalent and Divalent Rare Earth Thiocyanate Complexes Synthesised by Redox Transmetallation. *Eur. J. Inorg. Chem.* **2010**, *2010*, 2813–2825. [CrossRef]
38. Leung, W.-P.; Chan, Y.-C.; Mak, T.C.W. Synthesis and Structural Characterization of Thiophosphinoyl Late-Transition-Metal and Divalent Lanthanide Complexes Derived from 2-Quinolyl-Linked (Thiophosphorano)methane. *Eur. J. Inorg. Chem.* **2013**, *2013*, 6103–6110. [CrossRef]
39. Burin, M.E.; Pushkarev, A.P.; Fukin, G.K.; Rumyantsev, R.V.; Konev, A.N.; Bochkarev, M.N. Synthesis of EuS and EuSe Particles via Thermal Decomposition of Dithio- and Diselenophosphinate Europium Complexes. *Nanotechnol. Russ.* **2017**, *12*, 66–72. [CrossRef]
40. Silantyeva, L.I.; Ilichev, V.A.; Shavyrin, A.S.; Yablonskiy, A.N.; Rumyantcev, R.V.; Fukin, G.K.; Bochkarev, M.N. Unexpected Findings in a Simple Metathesis Reaction of Europium and Ytterbium Diiodides with Perfluorinated Mercaptobenzothiazolates of Alkali Metals. *Organometallics* **2020**, *39*, 2972–2983. [CrossRef]
41. Stewart, O.C., Jr.; Marwitz, A.C.; Swanson, J.; Bertke, J.A.; Hartman, T.; Monteiro, J.H.S.K.; de Bettencourt-Dias, A.; Knope, K.E.; Stoll, S.L. Lanthanide Luminescence and Thermochromic Emission from Soft-Atom Donor Dichalcogenoimidodiphosphinate Ligands. *Inorg. Chem.* **2022**, *61*, 15547–15557. [CrossRef] [PubMed]
42. Bokouende, S.S.; Ward, C.L.; Allen, M.J. Understanding the Coordination Chemistry and Structural and Photophysical Properties of $Eu^{II}$- and $Sm^{II}$-Containing Complexes of Hexamethylhexacyclen and Noncyclic Tetradentate Amines. *Inorg. Chem.* **2024**, *63*, 16991–17004. [CrossRef]
43. Ostrosablin, A.N.; Ilichev, V.A.; Rogozhin, A.F.; Kuznetsova, O.V.; Dorovatovskii, P.V.; Rumyantcev, R.V.; Fukin, G.K.; Bochkarev, M.N. Synthesis and Structures of Eu(II) Complexes with Anionic Perfluoro-2-mercaptobenzothiazolate and Macrocyclic Ligands. *Inorg. Chim. Acta* **2026**, *590*, 122987. [CrossRef]
44. Berardini, M.; Emge, T.; Brennan, J.G. One-dimensional Coordination Polymers: [{(pyridine)$_2$Eu(μ-SeC$_6$H$_5$)$_2$}$_4$]$_n$ and [(THF)$_3$Eu(μ-SeC$_6$H$_5$)$_2$]$_n$. *J. Am. Chem. Soc.* **1993**, *115*, 8501–8502. [CrossRef]
45. Berardini, M.; Emge, T.; Breenan, J.G. Heterometallic Rare Earth/Group II Metal Chalcogenolate Clusters. *J. Am. Chem. Soc.* **1994**, *116*, 6941–6942. [CrossRef]
46. Berardini, M.; Emge, T.J.; Brennan, J.G. Lanthanide-Group 12 Metal Chalcogenolates: A Versatile Class of Compounds. *Inorg. Chem.* **1995**, *34*, 5327–5334. [CrossRef]
47. Lee, J.; Emge, T.J.; Brennan, J.G. Heterometallic Lanthanide−Group 14 Metal Chalcogenolates. *Inorg. Chem.* **1997**, *36*, 5064–5068. [CrossRef]
48. Goodwin, C.A.P.; Schlimgen, A.W.; Albrecht-Schönzart, T.E.; Batista, E.R.; Gaunt, A.J.; Janicke, M.T.; Kozimor, S.A.; Scott, B.L.; Stevens, L.M.; White, F.D.; et al. Structural and Spectroscopic Comparison of Soft-Se vs. Hard-O Donor Bonding in Trivalent Americium/Neodymium Molecules. *Angew. Chem. Int. Ed.* **2021**, *60*, 9459–9466. [CrossRef] [PubMed]
49. Cary, D.R.; Arnold, J. Synthesis and Characterization of Divalent Lanthanide Selenolates and Tellurolates. X-ray Crystal Structures of Yb[SeSi(SiMe$_3$)$_3$]$_2$(TMEDA)$_2$ and {Eu[TeSi(SiMe$_3$)$_3$]$_2$(DMPE)$_2$}$_2$μ-DMPE). *Inorg. Chem.* **1994**, *33*, 1791–1796. [CrossRef]
50. Khasnis, D.V.; Brewer, M.; Lee, J.; Emge, T.J.; Brennan, J.G. Rare Earth Phenyltellurolates: 1D Coordination Polymers. *J. Am. Chem. Soc.* **1994**, *116*, 7129–7133. [CrossRef]
51. Thiele, G.; Santner, S.; Donsbach, C.; Assmann, M.; Müller, M.; Dehnen, S. Solvothermal and Ionothermal Syntheses and Structures of Amine- and/or (Poly-)Chalcogenide Coordinated Metal Complexes. *Z. Krist.-Cryst. Mater.* **2014**, *229*, 489–495. [CrossRef]

52. Deka, R.; Dey, S.; Guo, Z.; Butcher, R.J.; Junk, P.C.; Turner, D.R.; Singh, H.B.; Deacon, G.B. Pushing the Boundary of Covalency in Lanthanoid-Tellurium Bonds: Insights from the Synthesis, Molecular and Electronic Structures of Low-Coordinate, Monomeric Europium(II) and Ytterbium(II) Tellurolates. *Chem. Eur. J.* **2023**, *29*, e202301054. [CrossRef]
53. Ding, Y.-S.; Jiang, X.-L.; Li, L.; Xu, C.-Q.; Li, J.; Zheng, Z. Atomically Precise Semiconductor Clusters of Rare-earth Tellurides. *Nat. Synth.* **2024**, *3*, 655–661. [CrossRef]
54. Li, L.; Ding, Y.-S.; Zheng, Z. Lanthanide-Based Molecular Magnetic Semiconductors. *Angew. Chem. Int. Ed.* **2024**, *63*, e202410019. [CrossRef] [PubMed]
55. Li, L.; Xue, T.-J.; Ding, Y.-S.; Zheng, Z. Rare-earth Chalcogenidotetrachloride Clusters ($RE_3ECl_4$, RE = Dy, Gd, Y; E = S, Se, Te): Syntheses and Materials Properties. *J. Mater. Chem. C* **2024**, *12*, 16506–16514. [CrossRef]
56. Huang, J.-Q.; Ding, Y.-S.; Zheng, Z. Triply Chalcogenophenolato-Bridged Erbium-Cyclooctatetraenyl Complexes: Syntheses and Single-Molecule Magnetic Properties. *Inorg. Chem. Front.* **2025**, *12*, 8560–8571. [CrossRef]
57. Wang, C. Efficient Reduction Method Enables Access to Rare-earth Telluride Clusters. *Commun. Chem.* **2024**, *7*, 96. [CrossRef]
58. Réant, B.L.L.; Seed, J.A.; Whitehead, G.F.S.; Goodwin, C.A.P. Uranium(III) and Uranium(IV) meta-Terphenylthiolate Complexes. *Inorg. Chem.* **2025**, *64*, 3161–3177. [CrossRef]
59. Starynowicz, P.; Bukietyńska, K.; Gołąb, S.; Ryba-Romanowski, W.; Sokolnicki, J. Europium(II) Complexes With Benzo-18-Crown-6. *Eur. J. Inorg. Chem.* **2002**, *2002*, 2344–2347. [CrossRef]
60. Starynowicz, P. Europium(II) Complexes with Unsubstituted Crown Ethers. *Polyhedron* **2003**, *22*, 337–345. [CrossRef]
61. Merzlyakova, E.; Wolf, S.; Lebedkin, S.; Bayarjargal, L.; Neumeier, B.L.; Bartenbach, D.; Holzer, C.; Klopper, W.; Winkler, B.; Kappes, M.; et al. 18-Crown-6 Coordinated Metal Halides with Bright Luminescence and Nonlinear Optical Effects. *J. Am. Chem. Soc.* **2021**, *143*, 798–804. [CrossRef]
62. Poe, T.N.; Molinari, S.; Justiniano, S.; McLeod, G.M.; Albrecht-Schönzart, T.E. Structural and Spectroscopic Analysis of Ln(II) 18-crown-6 and Benzo-18-crown-6 Complexes (Ln = Sm, Eu, Yb). *Cryst. Growth Des.* **2022**, *22*, 842–852. [CrossRef]
63. Baldwin, J.; Brookfield, A.; Whitehead, G.F.S.; Natrajan, L.S.; McInnes, E.J.L.; Oakley, M.S.; Mills, D.P. Isolation and Electronic Structures of Lanthanide(II) Bis(trimethylsilyl)phosphide Complexes. *Inorg. Chem.* **2024**, *63*, 18120–18136. [CrossRef]
64. Pyykkö, P.; Atsumi, M. Molecular Single-Bond Covalent Radii for Elements 1–118. *Chem. Eur. J.* **2009**, *15*, 186–197. [CrossRef] [PubMed]
65. Ding, Y.-S.; Han, T.; Hu, Y.-Q.; Xu, M.; Yang, S.; Zheng, Y.-Z. Syntheses, Structures and Magnetic Properties of a Series of Mono- and Di-nuclear Dysprosium(III)-Crown-Ether Complexes: Effects of a Weak Ligand-Field and Flexible Cyclic Coordination Modes. *Inorg. Chem. Front.* **2016**, *3*, 798–807. [CrossRef]
66. Ding, Y.-S.; Blackmore, W.J.A.; Zhai, Y.-Q.; Giansiracusa, M.J.; Reta, D.; Vitorica-Yrezabal, I.; Winpenny, R.E.P.; Chilton, N.F.; Zheng, Y.-Z. Studies of the Temperature Dependence of the Structure and Magnetism of a Hexagonal-Bipyramidal Dysprosium(III) Single-Molecule Magnet. *Inorg. Chem.* **2022**, *61*, 227–235. [CrossRef]
67. Xu, W.-J.; Luo, Q.-C.; Li, Z.-H.; Zhai, Y.-Q.; Zheng, Y.-Z. Bis-Alkoxide Dysprosium(III) Crown Ether Complexes Exhibit Tunable Air Stability and Record Energy Barrier. *Adv. Sci.* **2024**, *11*, 2308548. [CrossRef]
68. Nazarov, M.; Brik, M.G.; Spassky, D.; Tsukerblat, B. Crystal Field Splitting of 5d States and Luminescence Mechanism in $SrAl_2O_4:Eu^{2+}$ Phosphor. *J. Lumin.* **2017**, *182*, 79–86. [CrossRef]
69. Joos, J.J.; Smet, P.F.; Seijo, L.; Barandiarán, Z. Insights into the Complexity of the Excited States of Eu-doped Luminescent Materials. *Inorg. Chem. Front.* **2020**, *7*, 871–888. [CrossRef]
70. Huang, W.; Upton, B.M.; Khan, S.I.; Diaconescu, P.L. Synthesis and Characterization of Paramagnetic Lanthanide Benzyl Complexes. *Organometallics* **2013**, *32*, 1379–1386. [CrossRef]
71. Dolomanov, O.V.; Bourhis, L.J.; Gildea, R.J.; Howard, J.A.K.; Puschmann, H. OLEX2: A Complete Structure Solution, Refinement and Analysis Program. *J. Appl. Crystallogr.* **2009**, *42*, 339–341. [CrossRef]
72. Sheldrick, G. SHELXT—Integrated space-group and crystal-structure determination. *Acta Crystallogr. Sect. A* **2015**, *71*, 3–8. [CrossRef] [PubMed]
73. Sheldrick, G. Crystal structure refinement with SHELXL. *Acta Crystallogr. Sect. C* **2015**, *71*, 3–8. [CrossRef] [PubMed]